Anal. Bioanal. Electrochem., Vol. 16, No. 4, 2024, 344-359
https://www.doi.org/ 10.22034/abec.2024.712922

Analytical & Bioanalytical Electrochemistry

Full Paper

A Sensitive Electrochemical Genosensor for the Detection of p53, a Tumor Suppressor Gene using A Simple Method for Tag-Free ssDNA Immobilization based on Ceria Nanoparticles

Mahboubeh Eskandari, and Farnoush Faridbod*

Center of Excellence in Electrochemistry, School of Chemistry, College of Science, University of Tehran, Tehran, Iran

*Corresponding Author, Tel.: +98-2161113813
E-Mail: faridbodf@ut.ac.ir

Received: 7 December 2023 / Received in revised form: 18 April 2024 / Accepted: 21 April 2024 / Published online: 30 April 2024

Abstract- A sensitive electrochemical genosensor was introduced and developed for a tumor suppressor gene, p53, detection. An Au screen-printed electrode coated with polyaniline film and ceria nanoparticles decorated on reduced graphene oxide was employed. To generate the genosensor, a suitable ssDNA probe sequence was immobilized on the modified surface of a screen-printed electrode without requiring any labeling or tagging moieties. The surface properties of the resulting electrodes were evaluated through scanning electron microscopy (SEM) and atomic force microscopy (AFM). The hybridization phenomena of the probe and its target sequence were followed by a differential pulse voltammetric signal of tris(bipyridine) ruthenium(II) chloride as an electrochemical probe. The detection limit was found 1.3 fM, and the DPV current was proportional to the logarithm of the p53 ssDNA concentration from 10 fM to 0.1 nM. The proposed genosensor showed excellent sensitivity, high selectivity, and reasonable reproducibility, which can be useful in future cancer diagnosis microdevice development.

Keywords- Tumor suppressor gene; Genosensor; Ceria Nanoparticles; Label-free immobilization; Biosensor

1. INTRODUCTION

The tumor suppressor gene, p53 is a well-known and useful cancer diagnostic biomarker. The p53 protein pathway is critical to the regulation of cell growth, cell cycle control, DNA repair, and cell apoptosis. The p53 protein is called the "guardian of the genome" because of its role in pausing the cell cycle for DNA repair or assuring the removal of cells with unrepairable DNA damage. Mutation in the p53 gene that causes indeed in around half of all human malignancies, leads cancer cells to grow and spread in the body. Hence, the development of innovative methods for detecting the p53 gene and its mutations is encouraged for cancer diagnosis [1-3].

Detection of specific sequences of genes is clinically important for medical early diagnoses [4,5]. The p53 gene is one of these important biomarkers. Various methods have been proposed for the determination of p53 up to now, including real-time PCR [6], peptide nucleic acid probe [7], fluorimetry [8], and chemiluminescence [9]. Besides, electrochemical methods are well-established tools for sequence-specific detection of p53, given their relative simplicity, outstanding sensitivity, high selectivity, small sizes, the possibility of hyphenating them with other devices, and portable applicability at point-of-use [10-13]. Among the electrochemical assays, biosensors designed based on screen-printed electrodes have found widespread applications due to, at least in part, their advantages of compact size, relatively inexpensive, as well as good reproducibility [14-27].

Many DNA electrochemical sensors function based on fixing an appropriate ssDNA probe sequence on a suitable transducer to distinguish their complementary target sequences through the hybridization phenomenon. These types of biosensors are called “genosensor”. In designing an efficient genosensor, immobilizing ssDNA probes on the electrode surface should be done by a simple, reproducible practical approach in which the non-specific binding sites are restricted. Adsorption methods and covalent bonding using avidin-biotin interactions and self-assembly reaction of thiolated sequence are examples of such methods. Among these, adsorption techniques offer the simplest and easiest routes since they do not require the use of chemical reagents and modifications of DNA probes [28,29]. Furthermore, in the case of long sequences, avoid the intertwining of the strands because their continuations are not free and suspended.

To improve biomolecule immobilization on electrode surfaces, reduce denaturation and loss of bioactivity, and improve sensitivity and selectivity, different types of nanomaterial and nanocomposites have been utilized [30-32]. Graphene oxide (GO) and its reduced form (rGO) are commonly used in the construction of biosensors due to their easy synthesis and unique characteristics such as vast surface areas, high biocompatibility, and remarkable electronic properties. These compounds are also used for immobilizing DNA on electrode surfaces, through non-covalent interactions (π-π stackings) between graphene oxide and DNA bases

[29,33-35]. The use of metal oxide nanomaterials decorated on reduced graphene oxide (rGO), on the other hand, extremely enhances biosensor performance.

Oxides of lanthanide series such as cerium, samarium, terbium, europium, and ytterbium appear more effective than general metal oxides. They are excellent, bio-compatible catalysts, with larger surface areas, which can improve the interaction and hence sensing ability of graphene. The nanoparticle-graphene interactions reduce the stacking of graphene sheets to each other and produce an attractive matrix that prevents the agglomeration of nanoparticles too [12,29,33,36]. To better stack on the electrode surface, these nanocomposites have been placed on conducting polymers such as polyaniline (PANI) which has been among the most frequently used conducting polymers in developing biosensors [37-39].

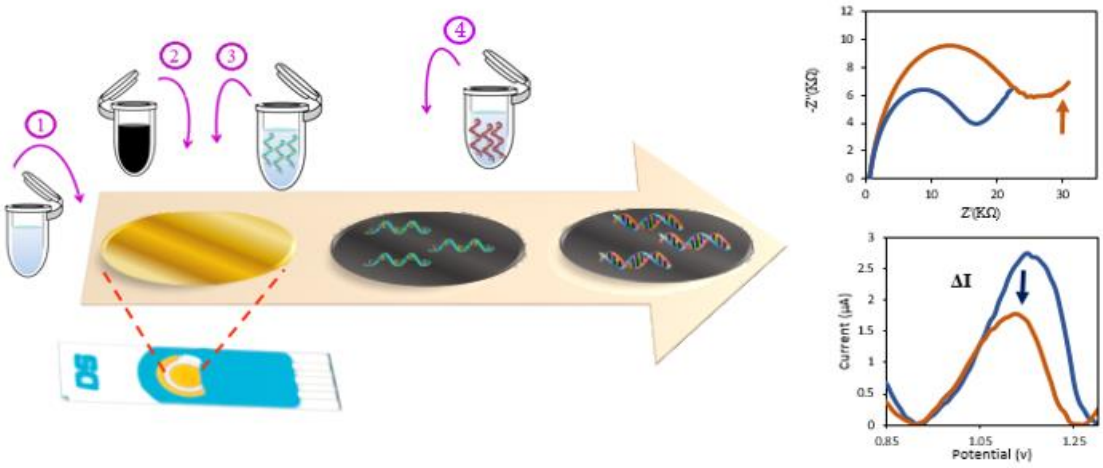

Scheme 1. Schematic process of preparing the proposed genosensor, where (1) is PANI, (2) is the CeO_2 NPs-rGO nanocomposite, (3) is the probe ssDNA solution in Tris-HCl buffer, and (4) represents the target ssDNA solution in Tris-HCl buffer

In this study, a genosensor was developed for the sensitive analysis of a specific sequence of the p53 tumor suppressor gene. A simple and label-free immobilization method using cerium oxide nanoparticles (CeO_2 NPs) and reduced graphene oxide was employed. A CeO_2 NPs-rGO and PANI were combined for the modification of the surface of a gold screen-printed electrode to create efficient adsorption. The hybridization of the ssDNA probe with its complementary target at the surface of the resulting electrode was assessed by following the tris(bipyridine) ruthenium(II) chloride $[Ru(bpy)_3]^{2+/3+}$ current signal of differential pulse voltammetry (DPV). The selectivity behavior of the proposed genosensor was studied using similar sequences with mismatched nucleotides. Scheme 1 shows the procedure for preparing the sensor and the electrochemical methods for hybridization detection.

2. EXPERIMENTAL SECTION

2.1. Chemicals

$[Ru(bpy)_3]Cl_2$), N_2H_4, $Ce(NO_3)_2{\cdot}6H_2O$, graphite flakes, ammonium peroxydisulfate ($(NH_4)_2S_2O_8$), tris(hydroxymethyl)aminomethane hydrochloride (Tris-HCl), ethylenediamine tetraacetic acid (EDTA), NaCl, NaOH, aniline ($C_6H_5NH_2$), and HCl were obtained from Merck-Sigma-Aldrich.

DNA primers with the below-specified sequences were purchased from Pishgam Biotechnology Company (Iran). TE buffer (10 mM Tris-HCl, EDTA 1 mM and pH=8.0) was used to prepare the stock solutions of DNA (10^{-4} M). This solution was stored at -20 °C.

ssDNA probe: 5′- GGCACAAACACGCACCTCAA-3′ [12,13]

Target sequence: 5′- TTGAGGTGCGTGTTTGTGCC-3′

Mismatch (3MM): 5′- TTGAGATGCGTATTTATGCC-3′

Non-complementary: 5′- GCCGACAATACAGGCTCAAG-3′

The DNA solution was diluted several times to prepare the 7.5 μM probe ssDNA solution. Various other solution concentrations of target ssDNA for calibration curve had been prepared with Tris-HCl buffer (10 mM) supplemented with NaCl (10 mM) pH=7.40. All solutions were prepared with deionized distilled water.

2.2. Devices and Measurements

A DropSens potentiostat was used in all electrochemical studies. The working electrode was a modified screen-printed gold electrode (SPGE). Cyclic voltammetry (CV) and electrochemical impedance spectroscopy (EIS) experiments were performed in a 0.01 M KCl electrolyte and 5 mM $K_3[Fe(CN)_6]/K_4[Fe(CN)_6]$ (1:1). EIS experiments were carried out in a frequency window ranging from 100 kHz to 0.1 Hz, while applying respective AC and DC voltages of 5 mV and 0.2 V *vs.* Ag/AgCl (saturated KCl), that was equal toward the open circuit voltage of this electrochemical setup**.**

Differential pulse voltammetry (DPV) experiments were conducted in an electrolyte of Tris-HCl 10 mM, and 10 mM NaCl (pH=7.40). During the tests, the electrode potential was scanned in the range of 0.7-1.3 V using a modulation amplitude of 25 mV and a modulation time of 50 ms. The solution was then changed with a 20 μM $[Ru(bpy)_3]^{2+/3+}$ solution in an identical Tris-HCl buffer under stirring for 5 minutes. Sequentially, the electrode was washed, and the DPV signal of cumulative $[Ru(bpy)_3]^{2+/3+}$ was recorded in the same buffer solution. The potential was altered from 0.6 to 1.3 V (*vs.* Ag/AgCl). All experiments were performed at room temperature.

The surface morphologies of rGO-CeO_2 and nano-PANI were studied via SEM on a Zeiss EVO LS10 SEM instrument. AFM, MultiMode 8 SPM with a NanoScope V control unit (Santa Barbara, Bruker AXS, CA, USA) was used for atomic force microscopy.

2.3. Synthesis of Polyaniline

Polyaniline (PANI) was produced using a previously described procedure [29,40]. Typically, 1.14 mL of aniline was added into a solution of HCl (50 mL, 1 M) at room temperature, while stirring. Afterwards, a 0.25 M ammonium peroxydisulfate solution (50 mL) as an oxidant agent was added to the aniline solution, and the resulting mixture was sonicated at 4 °C for 2 hours. After isolating the emerald green product, it was rinsed using water and 1 M HCl until it became colourless. The final product was dried for 24 hours at 60 °C.

2.4. Preparation of CeO2 NPs-rGO

CeO_2 NPs-rGO was prepared as described elsewhere [41]. This involved dissolving 1 mmol of $Ce(NO_3)_3.6H_2O$ in 30 mL of distilled water, followed by adding 2 mL of 20% NH_4OH aqueous solution in a dropwise manner for 1 hour, under sonication. Immediately, 60 mL of 0.5 mg mL^{-1} rGO suspension was added to this mixture. The resulting suspension was refluxed for 60 minutes, and the solid product was orderly isolated and repeatedly washed using ethanol and distilled water using centrifugation. The product was eventually dried at 60 °C for 24 hours.

2.5. Immobilization and hybridization of the probe DNA

The SPGE was initially polished using 1.0 μm alumina slurry, followed by 3 minutes of sonication in ultrapure water and drying under ambient conditions. Then 1 μL of 0.05 mg mL^{-1} of polyaniline dispersed in distilled water was dropped on the SPGE, and after drying, 1 μL of 0.5 mg mL^{-1} CeO_2 NPs-rGO (with 1:2 CeO_2: rGO mass ratio) was placed on the electrode surface and let dried at room temperature. This was followed by placing 1 μL of a solution of ssDNA probe (7.5 μM in 0.01 M Tris-HCl buffer) on the modified electrode and leaving the system for 1 hour without allowing it to dry. To remove any weakly attached ssDNA molecules, the surface of the electrode (ssDNA/ceria NPs-rGO/nano-PANI/SPGE) was rinsed using 0.01 M Tris-HCl buffer.

Finally, 1 μL of various concentrations solutions of the target ssDNA in 0.01 M Tris-HCl buffer was dropped on the ssDNA/ceria NPs-rGO/nano-PANI/SPGE electrode and the electrode was incubated at 37 °C for 60 minutes for the hybridization to proceed. The electrode was washed using the same Tris-HCl buffer solution to eliminate any un-hybridized target DNA.

2.6. Real sample analysis

Human blood plasma samples were used as real samples. For the analyses, to each fresh sample, 2 mL of 0.1 M nitric acid was first added, followed by centrifugation at 4000 rpm, for 20 minutes to isolate the protein content.

The supernatant was subsequently collected and diluted 50 folds using a solution of 10 mM of Tris-HCl, containing 10 mM NaCl (pH=7.40). Sequentially, the samples were spiked with various amounts of the target ssDNA, and the measurements were conducted by dropping 10 µL of the sample on the surface of the developed modified SPGE electrode.

3. RESULTS AND DISCUSSION

3.1. Structure and morphology evaluations

The structure and morphology of the modified surface of SPGE were studied by SEM and AFM. The SEM image of bare SPGE is shown in Figure 1A. The folded structure of the rGO sheets is well visible in Figure 1B. The SEM image in Figure 1C illustrates the typical globular morphology of nano-PANI. Figure 1D shows the modification of the SPGE with nano-PANI and ceria nanoparticles decorated rGO. The SEM images in Figures 1E and 1F illustrate the surface of the genosensor before and after the immobilization of ssDNA.

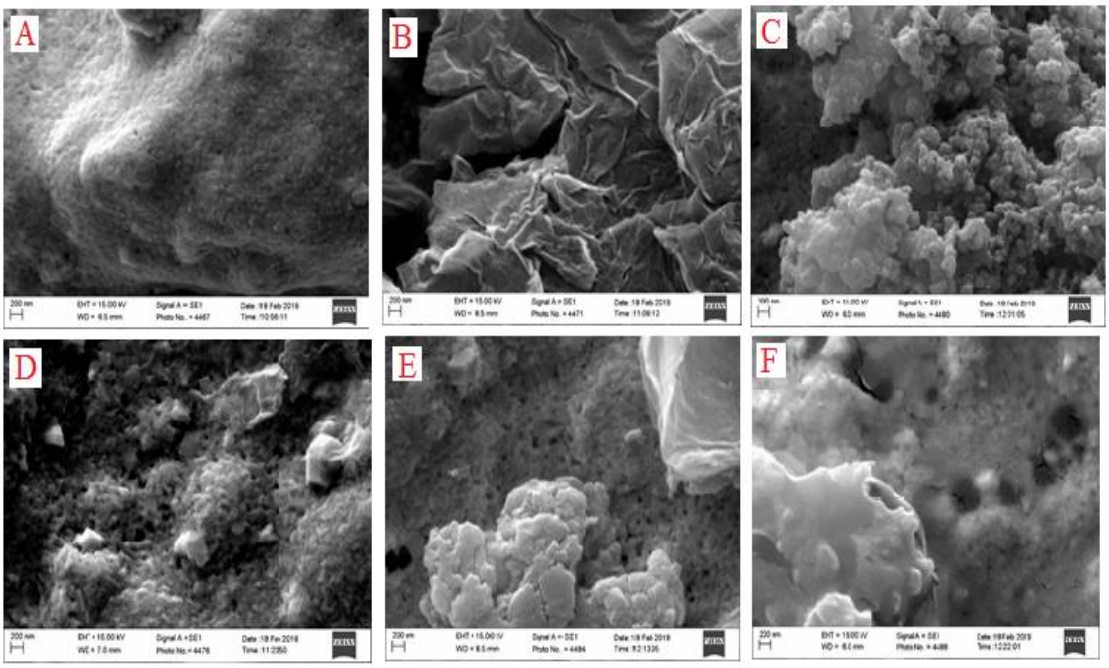

Figure 1. SEM image of (A) bare SPGE, (B) rGO, (C) nano-PANI, (D) nano-PANI/SPGE, (E) ceria NPs-rGO /nano-PANI/SPGE, (F) ssDNA/ceria NPs-rGO /nano-PANI/SPGE

Ceria or CeO_2 NP are one the most important nanomaterials that can adsorb DNA [42,43]. Due to the positive surface charge on the cerium NPs and the negative charge of the DNA

molecule, electrostatic interactions at the minor groove of the DNA sequence can occur. Also, phosphate groups on the DNA structure can adsorb on the oxygen vacancies of the cerium oxide nanoparticles. In this way, the DNA sequence can be immobilized on the electrode surface horizontally while their base moieties can enter a π-π interaction with rGO.

The AFM images (Figure 2) show that the bare SPGE is relatively smooth, but after modification with CeO_2 NPs-rGO, it has a completely different morphology, with a large number of hill-like peaks, and it is discovered that the CeO_2 NPs-rGO is homogeneous.

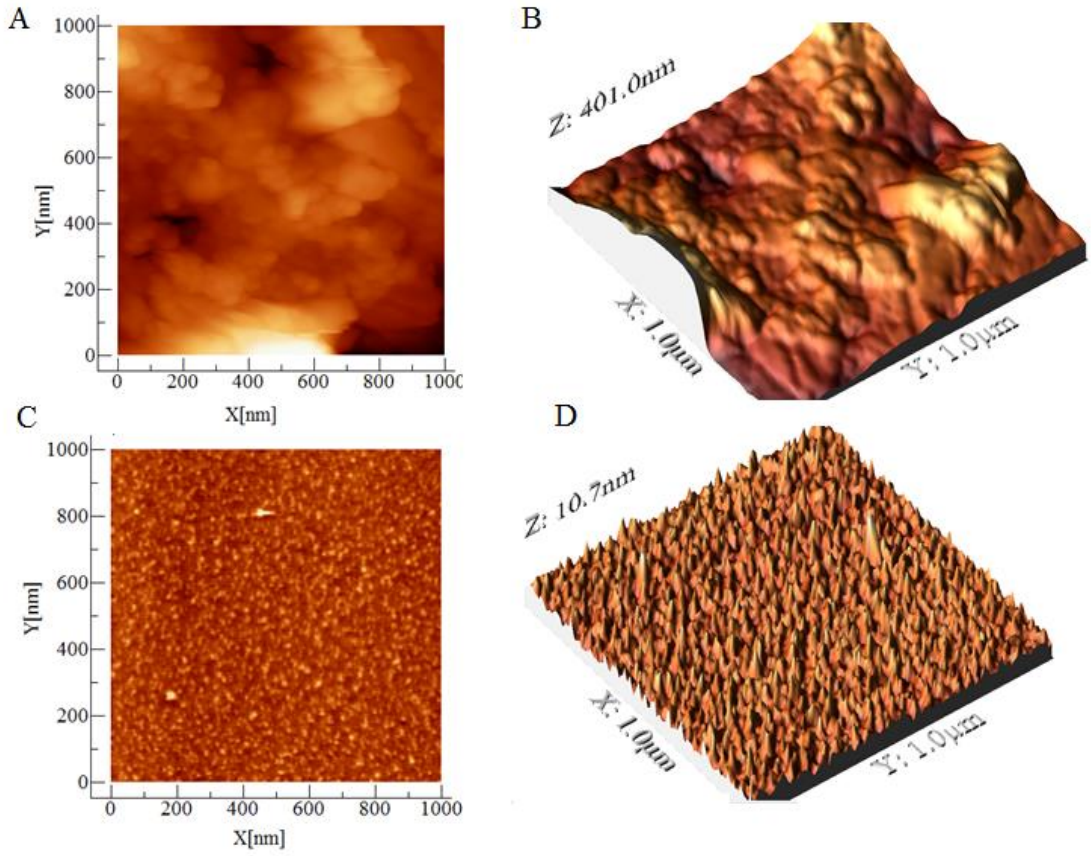

Figure 2. AFM images of (A) unmodified SPGE, (B) ceria NPs-rGO/nano-PANI/SPGE, (C) bare SPGE (three-dimension), (D) ceria NPs-rGO/nano-PANI/SPGE (three-dimension)

3.2. Electrochemical studies

The surface characteristics of the genosensor at various fabrication stages were investigated through CV and EIS analyses using $[Fe(CN)_6]^{3-/4-}$ as a redox probe [43]. Figure 3A illustrates the CVs obtained with the electrodes after performing various modifications of the SPGE. After modification with nano-PANI, CeO_2 NPs-rGO, immobilization of ssDNA probe, and hybridization with an ssDNA target, Figure 3A, CV b demonstrates that the deposition of CeO_2 NPs-rGO increased peak currents and diminished the peak separation (ΔE_p). This suggests that the use of both nano-PANI and CeO_2 NPs-rGO effectively improved the surface area. This

further increased the conductivity of the electrode, as well as enhanced the electron transfer phenomena between the probe and electrode. To do further, after successfully immobilizing the ssDNA probe on the modified electrode, a significant decrease was observed in the peak current (Figure 3A, curve c), since the immobilization of the ssDNA probe restricts the diffusion of $[Fe(CN)_6]^{3-/4-}$ onto the surface of the electrode surface, resulting in a reduction in peak currents.

Finally, the peak current further decreased (Figure 3A, curve d) after hybridization with the ssDNA target because of the additional insulation of the electrode induced by the double-stranded DNA.

EIS analyses were applied to monitor changes in the electrode upon each modification. The diameter of the semi-circular Nyquist plot at higher frequencies, reflects the electron-transfer resistance (R_{ct}), while the linear section of the plot at lower frequencies corresponds to the diffusion phenomena.

Predictably, after modifying the electrode surface with ceria NPs-RGO nanocomposite (Figure 3B, curve b), the value of R_{ct} decreased. Due to the favorable properties of the ceria NPs-rGO nanocomposite, including enhanced surface area and improved electron transfer properties, the R_{ct} values increased (Figure 3B, curves c and d) after immobilizing the ssDNA probe and hybridizing with ssDNA target on the electrode surface. This is the result of the electrostatic repulsion among the $[Fe(CN)_6]^{3-/4-}$ anions the negatively charged phosphate backbone of the DNA molecule [44,45].

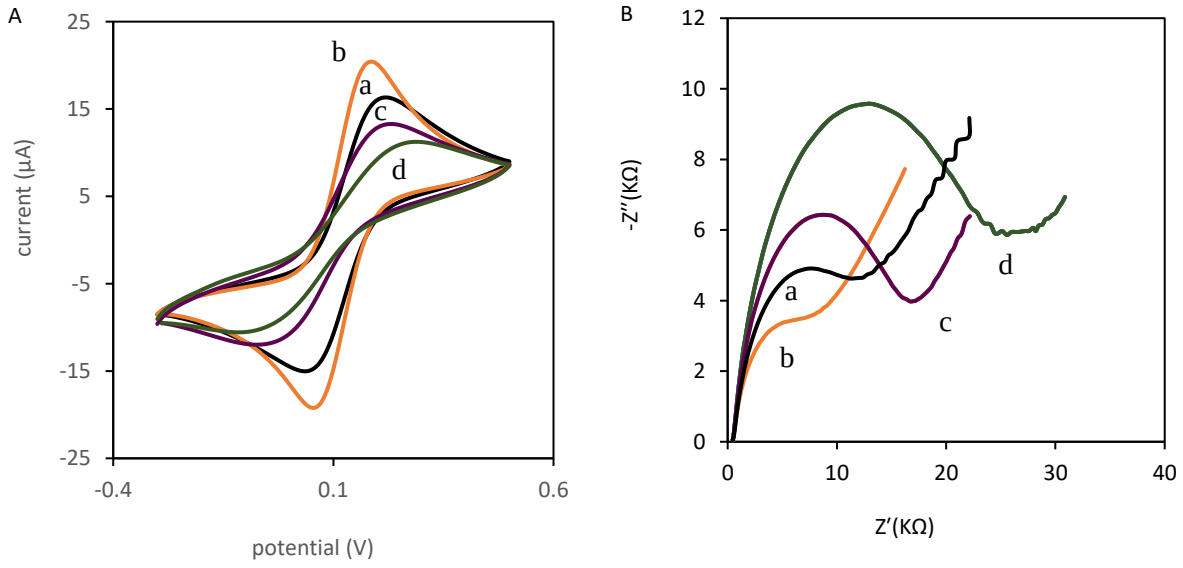

Figure 3. (A) Cyclic voltammograms and (B) Nyquist diagrams obtained in a 5 mM $[Fe(CN)_6]^{3-/4-}$ in 0.01 M KCl using (a) unmodified SPGE (b) ceria NPs-rGO/nano-PANI/SPGE (c) ssDNA/ceria NPs-rGO/nano-PANI/SPGE (d) ssDNA/ceria NPs-rGO/nano-PANI/SPGE hybridized with 1×10^{-10} M target DNA

3.3. Optimization

The concentration of ssDNA probe, hybridization time, and $[Ru(bpy)_3]^{2+/3+}$ concentration had a significant impact on the genosensor analytical performance. These factors were optimized as explained below.

The genosensor with 1, 2.5, 5, 7.5, 10, 12.5, and 15 µM of ssDNA probe onto the surface of the modified SPGE. The highest response of the genosensor occurred only at 5 µM and 7.5 µM concentrations of ssDNA probe. The response was a little bit higher at a 7.5 M concentration of the ssDNA probe, thus this concentration was finally selected as the optimum concentration.

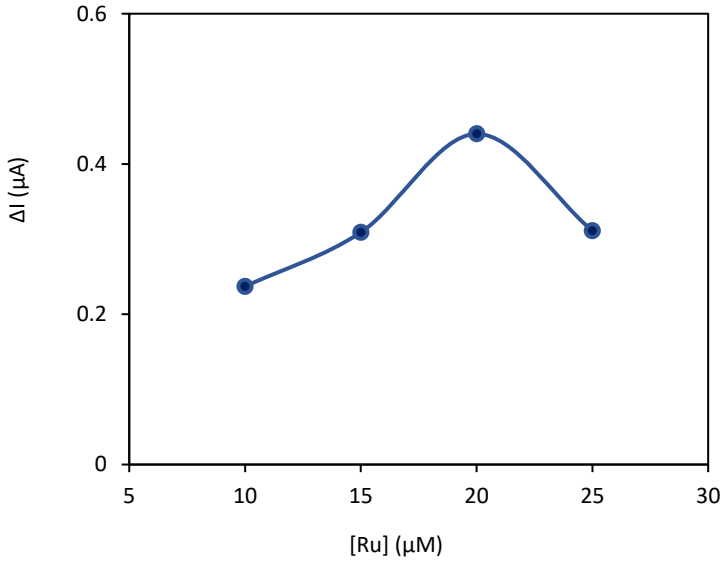

Figure 4. The influence of $[Ru(bpy)_3]^{2+/3+}$ concentration on biosensor response

The concentrations of $[Ru(bpy)_3]^{2+/3+}$ as a hybridization indicator were then optimized in the following step. Several concentrations of $[Ru(bpy)_3]^{2+/3+}$ were determined (10, 15, 20, and 25 µM). Figure 4 shows that a 20 µM concentration of $[Ru(bpy)_3]^{2+/3+}$ produced the highest response from the genosensor and was chosen as the optimal $[Ru(bpy)_3]^{2+/3+}$ concentration. The genosensor was designed and fabricated as shown in Scheme 1.

To confirm its response, various control experiments were done. Initially, the genosensor was fabricated without ssDNA immobilization or hybridization, in both of which cases the genosensor produced no significant response (Figure 5).

The modified SPGE was placed in a Tris-HCl buffer containing 20 µM $[Ru(bpy)_3]^{2+/3+}$ solution and the solution was stirred for 5 minutes for accumulation to proceed. Then, the electrode was washed and the differential pulse voltammetric signal for the accumulated $[Ru(bpy)_3]^{2+/3+}$ was determined in the same Tris-HCl buffer solution.

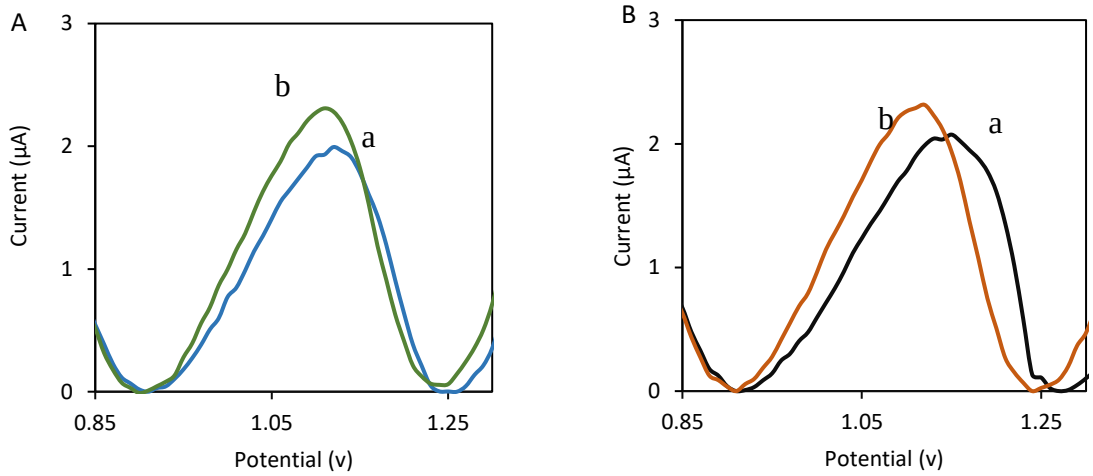

Figure 5. (A) DPV peak current recorded for 20 µM $[Ru(bpy)_3]^{2+/3+}$ using (a) ceria NPs-rGO/nano-PANI/SPGE, (b) ceria NPs-rGO/ nano-PANI/ SPGE hybridized with target ssDNA; (B) DPV peak current recorded for 20 µM $[Ru(bpy)_3]^{2+/3+}$ (a) ssDNA/ceria NPs-rGO/nano-PANI/SPGE (b) ssDNA/ ceria NPs-rGO/nano-PANI/SPGE without hybridization with target ssDNA

3.4. Analytical performance of the ssDNA target detection

The changes in the DPV peak currents recorded for identical $[Ru(bpy)_3]^{2+/3+}$ solutions before and after hybridization (ΔI) serve as a detection principle. Figure 6, clearly shows that the DPV peak current decreased after increasing the concentration of the ssDNA target, as formerly reported elsewhere [29,33]. Ru^{2+} in $[Ru(bpy)_3]^{2+/3+}$ that accumulates on the surface of ssDNA/ceria NPs-rGO/nano-PANI/SPGE genosensor. The guanine bases present in the ssDNA reduce Ru^{3+} in the absence of hybridization. However, hybridizing the ssDNA with its target sequence, leads to the inaccessibility of the guanine bases [46,47], making them less prone to the reaction of $[Ru(bpy)_3]^{2+/3+}$.

Subsequently, the formation of a DNA double helix further inhibits the reaction between the ssDNA guanine and $[Ru(bpy)_3]^{2+/3+}$, diminishing the DPV peak current of $[Ru(bpy)_3]^{2+/3+}$ when using the developed genosensor as the working electrode.

$$[Ru(bpy)_3]^{2+} \rightarrow [Ru(bpy)_3]^{3+} + e^- \quad (1)$$

$$[Ru(bpy)_3]^{3+} + DNA \rightarrow [Ru(bpy)_3]^{2+} + DNA_{ox} \quad (2)$$

The EIS data is in agreement with this event. After hybridizing the DNA, impedance increases, which reflects the formation of the double helix DNA, resulting in an enhanced repulsion between $[Fe(CN)_6]^{3-/4-}$ and the negative phosphate backbone of the DNA.

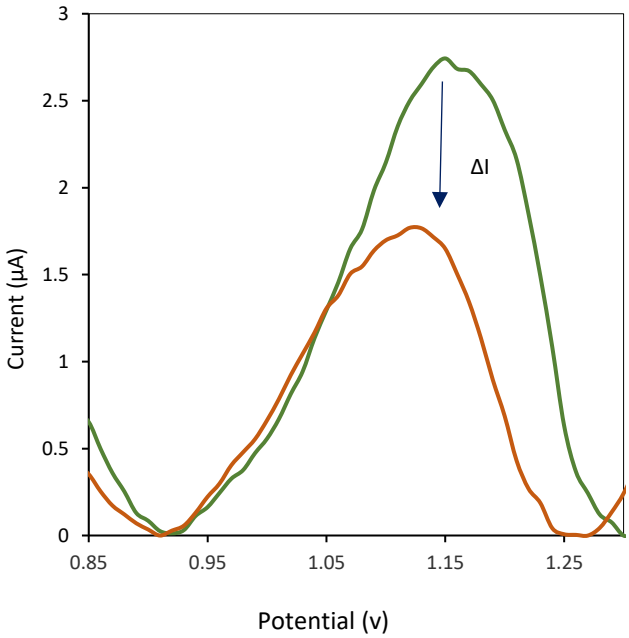

Figure 6. DPV peak current of 20 µM $[Ru(bpy)_3]^{2+/3+}$ recorded at (a) ssDNA/ceria NPs-rGO/nano-PANI/SPGE (b) ssDNA/ ceria NPs / nano-PANI/ SPGE hybridized with target ssDNA (concentration of sequences: 1×10^{-11} M) in Tris-HCl buffer (10 mM Tris-HCl, 10 mM NaCl and pH 7.4)

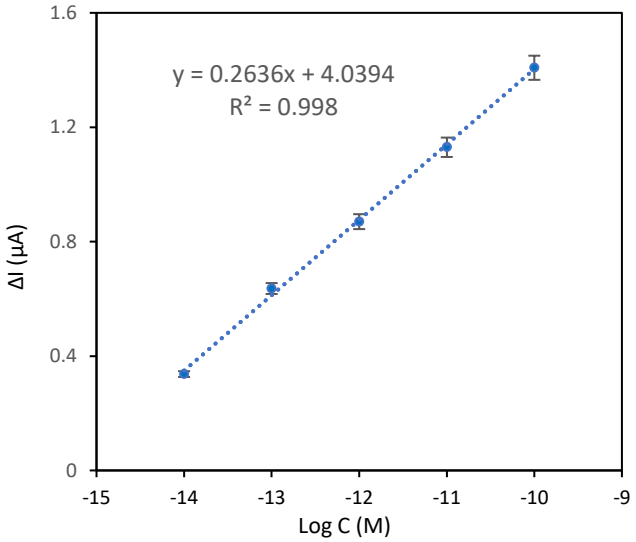

Figure 7. Calibration curve, the plot of ΔI versus the logarithm of target ssDNA concentration (M)

The genosensor was hybridized using various concentrations of ssDNA target for 1 hour under optimal conditions, and the resulting sensors were used in the DPV analyses in Tris-HCl buffer. According to Figure 7, the genosensor responses versus ssDNA target concentrations are in the range of 10^{-14} to 10^{-10} M. A logarithmic correlation exists between the response of the genosensor and the concentrations of the ssDNA target in the studied range. The limit of

detection (LOD) was 1.3 fM. The resulting linear equation was determined to be y = 0.2636 x + 4.0394 with a sensitivity of 26.36×10^{-2} μA/(μM) (R^2 = 0.998) and %RSD values was 5.2% (n= 4). The broad linear range and low LOD are satisfactory and comparable to previously reported p53 genosensors [10,12,13]. The sensitive genosensor performance is the result of the considerable surface/volume ratio, and electronic properties of graphene, together with the high surface area of ceria NPs.

3.5. Selectivity and reproducibility

By detecting three distinct target DNA sequences, the suggested electrochemical sensor's selective behavior was examined. A non-complementary sequence, three-base mismatched where mutations typically occur and a target sequence are the three target DNA sequences. Figure 8 and Figure 9 show the three-base mismatched strand displays smaller responses than the target ssDNA due to incomplete hybridization and the partial formation of the duplex of the three-base mismatched strands, but the non-complementary strand yields a small change in the response to the target ssDNA, demonstrating that hybridization did not occur. These revealed the excellent selectivity of the fabricated genosensors towards totally different ssDNA and some selectivity towards ssDNA that has few mismatches.

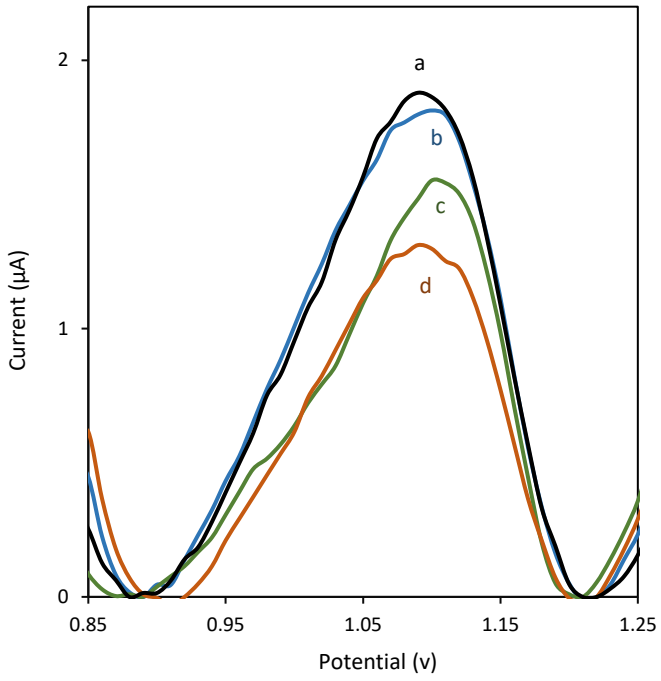

Figure 8. DPV peak current of 20 μM $[Ru(bpy)_3]^{2+/3+}$ at (a) ssDNA/ceria NPs-rGO/nano-PANI/SPGE, (b) ssDNA/ceria NPs/nano-PANI/SPGE hybridized with noncomplementary strand, (c) An electrode hybridized using a strand with three-base mismatch and (d) the electrode hybridized with target DNA (concentration of sequences: 1×10^{-11} M)) in Tris-HCl buffer

The optimal reproducibility of the response of the genosensor was evaluated using five ssDNA/ceria NPs-rGO/nano-PANI/SPGEs to analyze 1×10^{-13} M samples of target ssDNA. The relative standard deviation of five replicate analyses was 5.6%.

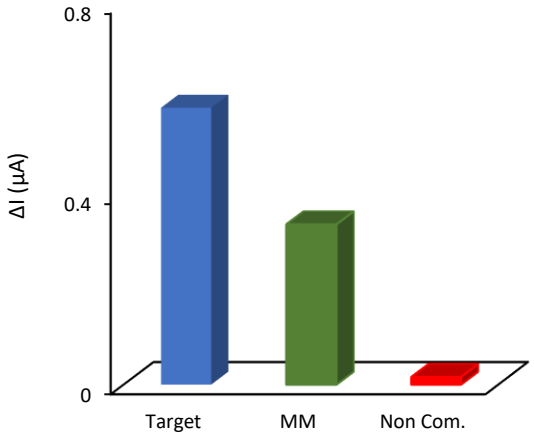

Figure 9. The response of the genosensor to different sequences (concentration of sequences: 1×10^{-11} M); MM: is a three-base mismatch strand, Non-Com (Noncomplementary strand): is a completely not matching ssDNA sequence

3.6. Analysis of the real sample

To test the applicability of the developed genosensor for the detection of the p53 gene in real sample analysis, the ssDNA/ceria NPs-rGO/nano-PANI/SPGE was used for the analysis of target ssDNA concentrations in human blood plasma. To this end, various concentrations of target ssDNA solution were spiked into the diluted human blood plasma after removing the protein content. The RSD values were determined to be 9.14% and 8.64%, for three electrodes in 10^{-13} M and 10^{-14} M of the target ssDNA sample. The observations confirmed the precision and reliability of the developed genosensor for the analysis of DNA in real samples. The total time takes the whole assay was done, including blood preparation, hybridization, and electrochemical measurements was about 2 hours. In a clinical diagnosis lab, this could be the appropriate time to perform a clinical analysis.

4. CONCLUSION

This study reports a sensitive electrochemical genosensor based on polyaniline and ceria NPs-rGO nanocomposite, which provides a biocompatible immobilization of probe ssDNA on the SPGE by physical adsorption and enhanced electron transfer. Tris(bipyridine)ruthenium(II) chloride $[Ru(bpy)_3]^{2+/3+}$ was used as the redox indicator. Using the described genosensor, high sensitivity and low detection limits, good selectivity, and the ability to discriminate mismatched strands from target ssDNA were observed. The entire assay sequence analysis including blood preparation, hybridization, and electrochemical measurements lasted about 2

hours, which should be further reduced for the device to be useful in diagnostic applications and clinical research.

Acknowledgments

The authors thank the research council of the University of Tehran for the financial support of this work.

Declarations of interest

The authors declare no conflict of interest in this reported work.

REFERENCES

[1] H.E. Marei, A. Althani, N. Afifi, A. Hasan, T. Caceci, G. Pozzoli, A. Morrione, A. Giordano, and C. Cenciarelli, Cancer Cell Int. 21 (2021) 703.
[2] B. Vogelstein, S. Sur, and C. Prives, Nature Education, 3 (2010) 6.
[3] G. Zhu, C. Pan, J.X. Bei, B. Li, C. Liang, Y. Xu, and X. Fu, Front. Oncol. 10 (2020) 595187.
[4] E.D. Esplin, L. Oei, M.P. Snyder, Pharmacogenomics 15 (2014) 1771.
[5] M. Smith, Proceeding Cautiously Front. Mol. Biosci. 4 (2017) 24.
[6] K. Will, G. Warnecke, S. Bergmann, W. Deppert, Nucleic Acids Research 23 (1995) 4023.
[7] J. Wang, G. Rivas, X. Cai, M. Chicharro, C. Parrado, N. Dontha, A. Begleiter, M. Mowat, E. Palecek, and P.E. Nielsen, Anal. Chim. Acta 344 (1997) 111.
[8] M. Hosseini, S. Mohammadi, Y.S. Borghei, and M.R. Ganjali, J. Fluorescence 27 (2017) 1443.
[9] L.M. Wang, X. Yao, X. Fang, and X. Yao, Applied Biochem. Biotechnol. 187 (2019) 152.
[10] E. Hamidi-Asl, J.B. Raoof, M.S. Hejazi, S. Sharifi, S.M. Golabi, I. Palchetti, and M. Mascini, Electroanalysis 27 (2015) 1378.
[11] P. Wang, H. Wu, Z. Dai, X. Zou, Chem. Commun. 48 (2012) 10754.
[12] R. Feng, X. Hu, C. He, X. Li, and X. Luo, Anal. Lett. 50 (2017) 336.
[13] X. Wang, X. Zhang, P. He, and Y. Fang, Biosens. Bioelectron. 26 (2011) 3608.
[14] M. Eskandari, and F. Faridbod, New Journal of Chem. 42 (2018) 15655.
[15] K. Yamanaka, M.C. Vestergaard, and E. Tamiya, Sensors 16 (2016) 1761.
[16] I.L. de Mattos, L. Gorton, and T. Ruzgas, Biosens. Bioelectron. 18 (2003) 193.
[17] C. Tortolini, V. Gigli, A. Angeloni, L. Galantini, F. Tasca, and R. Antiochia, Biosensors 13 (2023) 43.

[18] P. Norouzi, V.K. Gupta, F. Faridbod, M. Pirali-Hamedani, B. Larijani, and M.R. Ganjali, Anal. Chem. 83 (2011) 1564.
[19] S. Hassani, M.R. Akmal, A. Salek-Maghsoudi, S. Rahmani, M.R. Ganjali, P. Norouzi, and M. Abdollahi, Biosens. Bioelectron. 120 (2018) 122.
[20] P. Norouzi, F. Faridbod, B. Larijani, and M.R. Ganjali, Int. J. Electrochem. Sci. 5 (2010) 1213.
[21] K. Khoshnevisan, H. Baharifar, F. Torabi, M. Sadeghi Afjeh, H. Maleki, E. Honarvarfard, H. Mohammadi, S.M. Sajjadi-Jazi, S. Mahmoudi-Kohan, F. Faridbod, B. Larijani, F. Saadat, R. Faridi Majidi, and M.R. Khorramizadeh, Anal. Bioanal. Chem.413 (2021) 1615.
[22] K. Khoshnevisan, F. Torabi, H. Baharifar, S.M. Sajjadi-Jazi, M.S. Afjeh, F. Faridbod, B. Larijani, and M.R. Khorramizadeh, Anal. Bioanal. Chem. 412 (2020) 3615.
[23] L. Anvari, S.M. Ghoreishi, F. Faridbod, and M.R. Ganjali, Anal. Lett. 54 (2021) 2509.
[24] A. Shafaat, F. Faridbod, and M.R. Ganjali, New J. Chem. 42 (2018) 6034.
[25] F. Piroozmand, F. Mohammadipanah, and F. Faridbod, Synth. Syst. Biotechnol. 5 (2020) 293.
[26] P. Norouzi, B. Larijani, M.R. Ganjali, and F. Faridbod, Int. J. Electrochem. Sci. 7 (2012) 10414.
[27] K. Khoshnevisan, H. Maleki, E. Honarvarfard, H. Baharifar, M. Gholami, F. Faridbod, B. Larijani, R. Faridi Majidi, and M.R. Khorramizadeh, Microchim. Acta 186 (2019) 49.
[28] Y. Huang, J. Xu, J. Liu, X. Wang, and B. Chen, Sensors 17 (2017) 2375.
[29] N. Mohammadian, and F. Faridbod, Sens. Actuators B Chem 275 (2018) 432.
[30] M. Kaushik, S. Khurana, K. Mehra, N. Yadav, S. Mishra, and S. Kukreti, Curr. Pharm. Des. 24 (2018) 3697.
[31] M.R. Ganjali, H. Beitollahi, R. Zaimbashi, S. Tajik, M. Rezapour, and B. Larijani, Int. J. Electrochem. Sci. 13 (2018) 2519.
[32] V. Arabali, M. Ebrahimi, M. Abbasghorbani, V.K. Gupta, M. Farsi, M.R. Ganjali, and F. Karimi, J. Mol. Liq. 213 (2016) 312.
[33] S. Jafari, F. Faridbod, P. Norouzi, A.S. Dezfuli, and D. Ajloo, F. Mohammadipanah, and M.R. Ganjali, Anal. Chim. Acta 895 (2015) 80.
[34] A. Mohammadpour-Haratbar, S.B.A. Boraei, Y. Zare, K.Y. Rhee, and S.J. Park, Biosensors 13 (2023) 80.
[35] P.A. Rasheed, and N. Sandhyarani, Sens. Actuators B 204 (2014) 777.
[36] J. Gao, Y. Zhao, W. Yang, J. Tian, F. Guan, Y. Ma, J. Hou, J. Kang, and Y. Wang, Mater. Chem. Phys. 77 (2003) 65.
[37] J. Kappen, M. Skorupa, and K. Krukiewicz, Biosensors 13 (2023) 31.
[38] W. Yuan, X. Wang, Z. Sun, F. Liu, and D. Wang, Biosensors 13 (2023) 24.
[39] Z.A. Boeva, and V.G. Sergeyev, Polym. Sci. Ser. C 56 (2014) 144.

[40] S. Bhadra, D. Khastgir, N.K. Singha, and J.H. Lee, Progress in Polymer Science 34 (2009) 783.
[41] A.S. Dezfuli, M.R. Ganjali, P. Norouzi, and F. Faridbod, J. Mater. Chem. B 3 (2015) 2362.
[42] M. Kallur, M.N. Chandraprabha, H.K. Rajan, A. Khosla, and C. Manjunatha, ECS Trans. 107 (2022) 15935.
[43] R. Pautler, E.Y. Kelly, P.J. Huang, J. Cao, B. Liu, and J. Liu, ACS Appl. Mater. Interfaces 5 (2013) 6820.
[44] J.Y. Park, and S.M. Park, Sensors 9 (2009) 9513.
[45] I.I. Suni, TrAC Trends in Anal. Chem. 27 (2008) 604.
[46] M. Cui, Y. Wang, H. Wang, Y. Wu, and X. Luo, Sens. Actuators B 244 (2017) 742.
[47] S. Zhang, Y. Ding, and H. Wei, Molecules 19 (2014) 11933.